Organofluorine Binding to Sodium and Thallium(I) in Molecular Fluoroalkoxide Compounds

John A. Samuels, Emil B. Lobkovsky, William E. Streib, Kirsten Folting, John C. Huffman, Josef W. Zwanziger, and Kenneth G. Caulton*

Contribution from the Department of Chemistry and Molecular Structure Center, Indiana University, Bloomington, Indiana 47405

Received December 9, 1992

Abstract: The compounds $(NaOR_f)_4$ (R_f = $CH(CF_3)_2$), $Zr(OR_f)_4$ (**2**), $Zr(OR_f')_4$ (R_f' = $CMe(CF_3)_2$) (**3**), $Na_2Zr(OR_f)_6(C_6H_6)_n$ (**4a** when n = 1 and **4b** when n = 2), and $Tl_2Zr(OR_f)_6$ (**5**) have been synthesized and characterized by IR, multinuclear NMR, and mass spectrometry and (for **1**, **3**, **4a**,**b**, and **5**) X-ray diffraction structure determinations. The heavy fluorination of the molecular periphery makes all of these *molecular* compounds highly volatile. In addition, all X-ray structures (except that of **3**) show evidence of intramolecular ("secondary") bonding interactions between numerous organofluorines and the electrophiles sodium or thallium. The benzene in both solid compounds **4** forms a π-complex to sodium. The absence of benzene in **5** leads to additional *inter*molecular Tl–F interactions. The reality of these electrophile–F interactions is further supported by the fact that ^{205}Tl and ^{19}F NMR spectra show Tl–F coupling of a magnitude consistent with direct bonding. Moreover, variable-temperature ^{205}Tl and ^{19}F NMR studies reveal facile migration of both Tl electrophiles over the entire periphery of the $Zr(OR_f)_6$ octahedron. Cleavage of C–F bonds is evident in the electron impact mass spectra of these molecules, and especially from the fact that chemical vapor deposition of $(NaOR_f)_4$ onto silica at 285 °C gives NaF, not Na_2O. These ground-state metal–organofluorine interactions appear to provide a facile reaction channel for rupture of the strong C–F bond.

Introduction

Fluorocarbon derivatives of metal alkoxides and metal β-diketonates are attractive precursors for chemical vapor deposition (CVD) processing because of their generally greater volatility than that of their hydrocarbon analogues. This increased volatility may be due to intermolecular repulsions between the many fluorine lone pairs. Alternatively, the low polarizability of the fluorine may reduce the van der Waals attractive forces.[1] In reality, a combination of these effects, as well as previously unrecognized structural characteristics to be documented here, result in the high volatility of these materials. Purdy and others[2] have shown that an apparent consequence of volatility enhancement in β-diketonate systems by the use of organofluorine species is the incorporation of inorganic fluoride contamination in the CVD product. The occurrence of C–F bond cleavage is surprising, considering the strength of the C–F bond compared to C–O and C–H bond energies ($\Delta H°$ = 116, 88, and 99 kcal/mol, respectively).

In an investigation of substituted alkoxide-based precursors, an examination of the parent alcohols is relevant. Fluoro alcohols exhibit a variety of differences from their hydrocarbon analogues. They have relatively low pK_a's, many times lower than water (e.g., for $HOCH(CF_3)_2$, pK_a = 9.3), and are more sterically demanding than unsubstituted alcohols. The increased molecular weight of fluoro alcohols does not seem to affect their volatility since they usually have boiling points lower than those of the corresponding hydrocarbon systems, a phenomenon common to most fluorocarbon systems.[3] The stability of fluoro alcohols depends greatly on the degree of fluorination and the positions in which they are fluorinated. Fluoro-substituted alcohols can be readily converted to fluoroalkoxides[4] via methods analogous to those for hydrocarbon systems.

Beyond the investigation of fluorocarbon-based precursors, the interaction of covalently-bonded fluorine with electrophiles is of broad importance for its effect on chemical processes. Coordination of perfluorocarbons to photogenerated $Cr(CO)_5$[5] and interactions of alkali metals with fluorinated carboxylate and other biological substrates[6] have been documented. Ion-selective membrane transport of K^+ has also been shown to be influenced by pendant perfluorocarbon groups on benzene-18-crown-5,[7] and the coordination chemistry of progressively fluorinated cyclams[8] has been reported. Oxidative addition of an aromatic C–F bond to an electron-rich zero-valent tungsten center has also been shown to occur.[9] An extensive review of the interactions of halocarbons with metal centers and their effects on reaction chemistry is available.[10a] Interactions of electrophilic Zr(IV) with aryl fluorines in $B(Ar_f)_4^-$ are established[10b] in olefin polymerization catalysts. This report details structural and spectroscopic results of electrophile–organofluorine interactions relevant to the preference of C–F over C–O bond cleavage. These results also indicate that alkali metal fluoroalkoxides, like fluorinated β-diketonates, convert via CVD to metal fluorides instead of metal oxides.

Experimental Section

All manipulations were carried out under a dry nitrogen atmosphere using oven-dried glassware. Solvents were freshly distilled over sodium/benzophenone. Reagents were purchased from Aldrich with the exception of fluorinated alcohols, which were purchased from PCR. Tetraneopentylzirconium was prepared by literature methods.[11] Infrared spectra

(1) Reed, T. M., III. In *Fluorine Chemistry*; Simons, J. H., Ed.; Academic: New York, 1964; Vol. 5, p 133.

(2) (a) Purdy, A. P.; Berry, A. D.; Holm, R. T.; Fatemi, M.; Gaskill, D. K. *Inorg. Chem.* **1989**, *28*, 2799. (b) Zhao, J.; Dahmen, K.-H.; Marcy, H. O.; Tonge, L. M.; Marks, T. J.; Wessels, B. M.; Kannewurf, C. R. *Appl. Phys. Lett.* **1989**, *53*, 1750. (c) Larkin, D. L.; Interrante, L. V.; Bose, A. *J. Mater. Res.* **1990**, *5*, 2706.

(3) Banks, R. E.; Tatlow, J. C. In *Fluorine, The First Hundred Years*; Bank, R. E., Sharp, D. W. A., Tatlow, J. C., Eds.; Elsevier: New York, 1986; p 249.

(4) Willis, J. C. *Coord. Chem. Rev.* **1988**, *88*, 133.

(5) Bonneau, R.; Kelly, J. M. *J. Am. Chem. Soc.* **1980**, *102*, 1220.

(6) Murry-Rust, P.; Stallings, W. C.; Monti, C. T.; Preston, R. K.; Glusker, J. P. *J. Am. Chem. Soc.* **1983**, *105*, 3206.

(7) Shinkai, S.; Torigoe, K.; Manabe, O.; Kajiyama, T. *J. Am. Chem. Soc.* **1987**, *109*, 4458.

(8) Kimura, E.; Shionoya, M.; Okamoto, M.; Nada, H. *J. Am. Chem. Soc.* **1988**, *110*, 3679.

(9) Richmond, T. G.; Osterberg, C. E.; Arif, A. M. *J. Am. Chem. Soc.* **1987**, *109*, 8091.

(10) (a) Kulawiec, R. J.; Crabtree, R. H. *Coord. Chem. Rev.* **1990**, *99*, 89. (b) Bochmann, M. *Angew. Chem., Int. Ed. Engl.* **1992**, *31*, 1181. (c) For related work on CVD with $NaOCH(CF_3)_2$, see: Lingy, L. J.; Berry, A. D.; Purdy, A. P.; Ewing, K. J. *Thin Solid Films* **1992**, *209*, 9.

0002-7863/93/1515-5093$04.00/0

Table I. Crystallographic Data

	$(NaOCH(CF_3)_2)_4$	$Zr(OCMe(CF_3)_2)_4$	$Na_2Zr(OCH(CF_3)_2)_6(C_6H_6)_2$	$Na_2Zr(OCH(CF_3)_2)_6(C_6H_6)$	$Tl_2Zr(OCH(CF_3)_2)_6$
chemical formula	$C_{12}H_4F_{24}Na_4O_4$	$C_{16}H_{12}F_{24}O_4Zr$	$C_{30}H_{18}O_6F_{36}Na_2Zr$	$C_{24}H_{12}F_{36}Na_2O_6Zr$	$C_{18}H_6F_{36}O_6Tl_2Zr$
a, Å	10.648(1)	16.321(6)	16.783(4)	10.440(3)	19.879(2)
b, Å	9.936(1)	10.856(3)	14.927(4)	10.440(3)	10.182(1)
c, Å	11.315(1)	31.023(12)	9.667(2)	10.440(3)	20.456(1)
α, deg				106.20(2)	
β, deg	91.40(0)	104.74(1)	112.78(1)	112.78(1)	122.97(0)
γ, deg				106.20(2)	
V, Å^3	1196.63	5315.81	2232.79	966.21	3473.43
Z	2	8	2	1	4
fw	760.08	815.45	1295.61	1217.50	1502.14
space group	$P2_1$	$P2_1/n$	$C2/m$	$R\bar{3}$	$C2/c$
T, °C	−181	−174	−172	−170	−172
λ, Å	0.71069	0.71069	0.71069	0.71069	0.71069
ρ_{calcd}, g cm^{-3}	2.110	2.038	1.927	2.089	2.873
Mo K_α, μm^{-1}	3.18	5.9	4.5	5.1	98.6
R	.0268	.1314	.0627	.0280	.0481
R_w	.0308	.1343	.0573	.0264	.0497

were run on a Nicolet 510P FT-IR and a Perkin-Elmer 283 grating IR as KBr pellets. NMR spectra were run on a Nicolet NT-360 spectrometer (^{19}F, ^1H, and ^{205}Tl spectra at 340, 361, and 208 MHz, respectively). Samples were run in C_6D_6 and C_6F_6 with external references when necessary (^{19}F-F_3CCOOH (neat) = −78.45 ppm, ^1H residual protons in C_6D_6 = 7.15 ppm, 0.3 M aqueous $TlNO_3$ = 0.0 ppm). Elemental analyses were performed by Oneida Research Services. R_f = $CH(CF_3)_2$. R_f' = $CMe(CF_3)_2$. Sublimation results under 1 atm of pressure represent TGA observations under flowing helium.

$NaOR_f$ (1). Sodium hydride (0.96 g, 40 mmol) was suspended in 60 mL of Et_2O. To this was added dropwise 4.0 mL (38 mmol) of hexafluoroisopropyl alcohol. After gas evolution had ceased, the reaction mixture was stirred for an additional 30 min and filtered, and the solvent was removed from the filtrate *in vacuo*. The resulting oily colorless solid was recrystallized from hot (80 °C) toluene to give long rod-shaped crystals. Yield: 6.86 g (95%). ^1H NMR (25 °C): δ 4.12 (in C_6F_6), 4.12 (in d_8-toluene) (sept, J = 6.5 Hz). ^{19}F NMR (25 °C): δ −83.4 (in C_6F_6), −79.8 (in d_8-toluene) (d, J = 6.5 Hz). IR: 2834 (w), 1373 (m), 1277 (s), 1250 (m), 1231 (sh), 1196 (s), 1166 (s), 1122 (sh), 1094 (s), 1076 (s), 882 (m), 845 (m), 737 (m), 687 (m), 621 (w), 527 (w), 517 (w), 418 (w) cm^{-1}. Anal. Calcd for C_3HOF_6Na: C, 18.96; H, 0.53; F, 59.99. Found: C, 18.90; H, 0.48; F, 56.90.

CVD of $NaOR_f$. ($NaOR_f$) (0.509 g, 2.63 mmol) was loaded into a glass sample chamber and attached to the glass reactor chamber containing prepared glass plate substrates and fitted with a cold trap downstream (see Figure 2 for diagram). The system was evacuated to 10^{-2} Torr and the reactor heated to 285 °C for 2 h to remove any moisture. The cold trap was then filled with N_2(l), and the sample chamber was heated to 75 °C where, over a period of 6 h, **1** sublimed and an off-white iridescent coating was deposited in the reactor chamber. Upon completion of the deposition, the contents of the cold trap were vacuum transferred to a prepared NMR tube. Anal. (coating) Calcd for NaF: C, 0.00; F, 45.25. Found: C, 0.54; F, 47.49.

$TlOR_f$. Thallium(I) ethoxide (4.99 g, 20.0 mmol) was placed in 40 mL of anhydrous ethanol containing 5.0 mL (47.4 mmol) of hexafluoroisopropyl alcohol. The mixture was stirred for 3 h. The solvent was then removed *in vacuo*. Remaining solid was sublimed at 80 °C at 10^{-2} Torr. Yield: 5.94 g (80%). ^1H NMR (C_6D_6): δ 4.70 (sept, $^3J_{H-F}$ = 6.8 Hz). ^{19}F NMR (C_6D_6): δ −77.0 (br, s).

$Zr(OR_f)_4$ (2). Zr(neopentyl)$_4$ (0.50 g, 1.33 mmol) was dissolved in 30 mL of toluene at 0 °C. To this was added dropwise 0.93 g (5.55 mmol, 0.59 mL) of hexafluoroisopropyl alcohol via syringe. The reaction mixture was allowed to come to room temperature and stir for 30 min, during which time a colorless solid precipitated. The solution was warmed to dissolve the solid and allowed to return to room temperature. The solvent was removed *in vacuo*, and the resulting white solid was sublimed at 60 °C at 10^{-2} Torr. Yield: 0.82 (80%). ^1H NMR (C_6F_6, 25 °C): δ 4.79 (br, sept, J_{H-F} = 5.4 Hz). ^{19}F NMR (C_6F_6): δ −77.3 (br, s). IR: 2932 (w), 1372 (m), 1298 (m), 1292 (vs), 1181 (vs), 1122 (sh), 1105 (m), 895 (m), 864 (sh), 849 (m), 750 (m), 689 (m), 538 (m), 521 (m) cm^{-1}. Anal. Calcd for $C_{12}H_4O_4F_{24}Zr$: C, 18.96; H, 0.53. Found: C, 18.53; H, 0.49.

$Zr(OR_f')_4$ (3). A preparation identical to that for $Zr(OR_f)_4$ was followed using 0.20 g (0.53 mmol) of Zr(neopentyl)$_4$ and 0.500 g (2.75 mmol, 0.34 mL) of $R_f'OH$. The product sublimed at 45 °C at 10^{-2} Torr. Yield: 0.32 g (74%). ^1H NMR (C_6F_6): δ 1.54 (s). ^{19}F NMR (C_6F_6): δ −82.9 (s). IR: 3020 (w), 2964 (w), 1460 (w), 1390 (w), 1312 (m), 1217 (s), 1177 (s), 1123 (m), 1086 (s), 1003 (m), 874 (w), 781 (m), 716 (w), 702 (m), 619 (w), 540 (w), 505 (w), 436 (w) cm^{-1}. Anal. Calcd for $C_{16}H_{12}O_4F_{24}Zr$: C, 23.57; H, 1.49; F, 55.94. Found: C, 23.51; H, 1.34; F, 53.29.

$Na_2Zr(OR_f)_6(C_6H_6)_x$ (X = 1, 2) (4a,b). Method 1: $ZrCl_4$ (0.41 g, 1.75 mmol) and $NaOR_f$ (2.00 g, 10.5 mmol) were suspended in 50 mL of toluene. The reaction mixture was refluxed for 24 h. The solvent was then removed, and the remaining white solid was sublimed at 80 °C at 10^{-2} Torr for 4 h to remove any remaining $NaOR_f$. The remaining white solid was then sublimed for 8 h at 110 °C at 10^{-2} Torr giving $Na_2Zr(OR_f)_6$. Recrystallization from hot benzene gave $Na_2Zr(OR_f)_6(C_6H_6)_x$. Yield: 0.96 g (48%).

Method 2: $Zr(OR_f)_4$ (0.25 g, 0.33 mmol) and $NaOR_f$ (0.125 g, 0.66 mmol) were suspended in 20 mL of benzene. The reaction mixture was then heated to reflux for 3 h. The solution was allowed to cool slowly to 25 °C, producing octahedral and prismatic colorless crystals of $Na_2Zr(OR_f)_6(C_6H_6)_x$ (x = 1, 2). Drying of crystals *in vacuo* gave $Na_2Zr(OR_f)_6$. Yield: 0.35 g (92%). ^1H NMR (25 °C): δ 4.63 (in C_6F_6), 4.81 (in C_6D_6) (br, sept, $^3J_{H-F}$ = 3.7 Hz). ^{19}F NMR (25 °C): δ −80.15 (in C_6F_6), −78.0 (in C_6D_6) (br, d, $^3J_{H-F}$ = 3.7 Hz). IR: 2964 (w), 2919 (w), 1372 (m), 1359 (sh), 1281 (m), 1251 (m), 1235 (s), 1217 (sh), 1177 (vs), 1098 (m), 884 (w), 847 (m), 749 (m), 687 (m), 666 (w), 531 (w), 521 (w), 455 (w) cm^{-1}. Anal. Calcd for $C_{18}H_6O_6F_{36}ZrNa_2$: C, 18.97; H, 0.53; F, 60.03. Found: C, 19.09; H, 0.53; F, 57.38.

$Tl_2Zr(OR_f)_6$ (5). $Zr(OR_f)_4$ (0.25 g, 0.33 mmol) and $TlOR_f$ (0.244 g, 0.66 mmol) were suspended in 20 mL of toluene. The solution was heated to reflux for 20 min and allowed to cool slowly to give colorless rods. The solvent was filtered off, and the crystals were dried *in vacuo*. Yield: 0.48 g (95%). ^1H NMR (C_6F_6, 25 °C): δ 4.90 (m). ^{19}F NMR (C_6F_6, 25 °C): fluxional pattern at δ −77.8 (distorted triplet, $^1J_{Tl-F}$ = 383.9 Hz). IR: 2961 (w), 2934 (w), 1372 (m), 1358 (w), 1281 (s), 1254 (s), 1229 (s), 1218 (sh), 1181 (s), 1161 (s), 1100 (m), 885 (m), 847 (m), 802 (w), 748 (m), 687 (m), 664 (w), 530 (w), 521 (m) cm^{-1}. Anal. Calcd for $C_{18}H_6O_6F_{36}ZrTl_2$: C, 14.39; H, 0.40; F, 45.53. Found: C, 14.41; H, 0.41; F, 44.09.

X-ray Structure Determination of $(NaOCH(CF_3)_2)_4$. A suitable single crystal (grown by slow vacuum sublimation within a sealed ampule) was selected using inert atmosphere handling techniques. The crystal was transferred to the goniostat, where it was cooled to −180 °C for characterization and data collection.[12] A systematic search of a limited hemisphere of reciprocal space yielded a set of reflections which exhibited monoclinic ($2/m$) Laue symmetry. The only systematic extinction observed was that of $0k0$ for $k = 2n + 1$. The choice of the non-centrosymmetric space group $P2_1$ was confirmed by the successful solution and refinement of the structure. Data collection ($6° < 2\theta < 55°$) was undertaken as detailed in Table I. The crystal diffracted extremely well. Plots of the four standard reflections measured every 300 reflections showed no systematic trends. No absorption correction was carried out. The structure was solved using the direct methods

(11) Davidson, P. J.; Lappert, M. F.; Pearce, R. *J. Organomet. Chem.* **1973**, *57*, 269.

(12) For a general description of diffractometer and crystallographic procedures, see: Huffman, J. C.; Lewis, L. N.; Caulton, K. G. *Inorg. Chem.* **1980**, *19*, 2755.

Table II. Selected Bond Distances (Å) and Angles (deg) for $(NaOCH(CF_3)_2)_4$ (1)

	Na(1)–O(5)	2.3163(18)	O(5)–Na(1)–O(25)	88.13(7)
	Na(1)–O(25)	2.3254(23)	O(5)–Na(1)–O(35)	90.57(7)
	Na(1)–O(35)	2.2637(19)	O(25)–Na(1)–O(35)	89.88(8)
	Na(2)–O(5)	2.2504(23)	O(5)–Na(2)–O(15)	89.52(8)
	Na(2)–O(15)	2.2962(20)	O(5)–Na(2)–O(25)	91.54(8)
	Na(2)–O(25)	2.2548(21)	O(15)–Na(2)–O(25)	89.44(8)
	Na(3)–O(5)	2.3147(20)	O(5)–Na(3)–O(15)	88.63(8)
	Na(3)–O(15)	2.2681(23)	O(5)–Na(3)–O(35)	89.69(7)
	Na(3)–O(35)	2.3009(21)	O(15)–Na(3)–O(35)	90.74(8)
	Na(4)–O(15)	2.3422(22)	O(15)–Na(4)–O(25)	86.89(7)
	Na(4)–O(25)	2.3149(21)	O(15)–Na(4)–O(35)	88.11(8)
	Na(4)–O(35)	2.3342(24)	O(25)–Na(4)–O(35)	88.43(8)
A	Na(1)–F(32)	2.641(2)	Na(1)–O(5)–Na(2)	90.33(8)
B	Na(1)–F(12)	2.831(2)	Na(1)–O(5)–Na(3)	89.04(7)
	Na(1)–F(10)	2.922(2)	Na(1)–O(5)–C(6)	118.30(16)
	Na(1)–F(30)	3.009(2)	Na(2)–O(5)–Na(3)	90.90(8)
	Na(1)–F(39)	3.447(2)	Na(2)–O(5)–C(6)	137.38(15)
C	Na(2)–F(23)	2.652(2)	Na(3)–O(5)–C(6)	118.39(15)
	Na(2)–F(8)	2.993(2)	Na(2)–O(15)–Na(3)	90.93(8)
	Na(2)–F(33)	3.379(2)	Na(2)–O(15)–Na(4)	90.96(7)
	Na(2)–F(24)	3.750(2)	Na(2)–O(15)–C(16)	122.80(16)
D	Na(3)–F(14)	2.635(2)	Na(3)–O(15)–Na(4)	90.83(8)
E	Na(3)–F(44)	2.636(2)	Na(3)–O(15)–C(16)	126.64(17)
	Na(3)–F(19)	3.471(2)	Na(4)–O(15)–C(16)	124.37(17)
F	Na(4)–F(29)	2.698(2)	Na(1)–O(25)–Na(2)	89.99(8)
G	Na(4)–F(18)	2.736(2)	Na(1)–O(25)–Na(4)	90.30(7)
H	Na(4)–F(38)	2.857(2)	Na(1)–O(25)–C(26)	115.80(16)
	Na(4)–F(43)	3.377(2)	Na(2)–O(25)–Na(4)	92.72(7)
	Na(4)–F(24)	3.506(2)	Na(2)–O(25)–C(26)	133.42(16)
			Na(4)–O(25)–C(26)	123.10(18)
			Na(1)–O(35)–Na(3)	90.69(7)
			Na(1)–O(35)–Na(4)	91.35(8)
			Na(1)–O(35)–C(36)	128.82(16)
			Na(3)–O(35)–Na(4)	90.23(8)
			Na(3)–O(35)–C(36)	121.69(16)
			Na(4)–O(35)–C(36)	123.44(17)

Table III. Distances Less than the Combined van der Waals Radii (Å) from Na to F Atoms of Neighboring Cubes in 1

I	Na(2)–F(9)	2.480(2)
J	Na(3)–F(22)	2.411(2)
K	Na(1)–F(28)	2.365(2)
	Na(3)–F(20)	2.745(2)
L	Na(4)–F(42)	2.805(3)
	Na(2)–F(8)	2.993(3)
	Na(4)–F(13)	3.375(3)
	Na(3)–F(12)	3.640(3)
	Na(1)–F(30)	3.736(3)

program SHELXS. All of the non-hydrogen atoms in the structure were located by SHELXS. Following initial refinement of the structure, all four hydrogen atoms were located. The full-matrix least-squares refinement was completed using anisotropic thermal parameters on all non-hydrogen atoms. The number of variables was 413, including the scale factor and an isotropic extinction parameter; the ratio of observations-to-variables was 2919/413 = 7.07. The final difference map was essentially featureless; the maximum peak was 0.21 e/Å^3. An attempt was made at determining the correct absolute structure for this non-centrosymmetric structure. Refinements of both enantiomers of this compound led to the same R values. The results of the structure determination are shown in Tables I, II and III and Figure 1.

X-ray Structure Determination of $Zr(OCMe(CF_3)_2)_4$. Crystals were grown by slow vacuum sublimation in a sealed ampule. The sample was first shown to undergo a phase transition at about −100 °C. An attempt to determine the structure with −90 °C data revealed the structure to be badly disordered with only the Zr and a tetrahedral set of oxygens being resolvable. A second sample was very carefully cooled through the phase transition, and it was then cooled to −174 °C for characterization and data collection ($6° < 2\theta < 45°$).[12] The unit cell doubled in size, and the space group changed from $P2_1/c$ to $P2_1/n$ on cooling. Following complete intensity data collection, data processing gave a residual of 0.062 for the averaging of 1858 unique intensities which had been observed more than once. Four standards measured every 300 data showed no significant trends. No correction was made for absorption. The structure was solved using a combination of direct methods (MULTAN78) and Fourier techniques. There are two molecules in the asymmetric unit. The positions

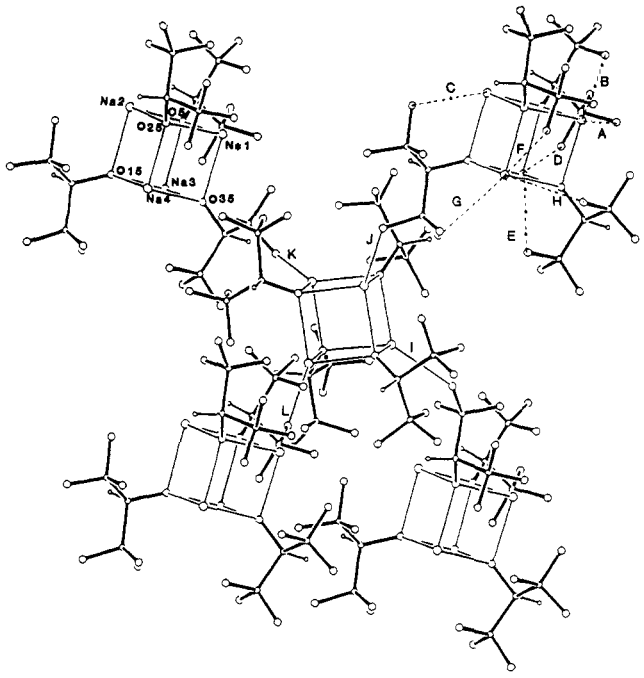

Figure 1. Ball-and-stick drawing of five molecular units of $(NaOCH(CF_3)_2)_4$ (1), showing selected atom labeling. Shortest intramolecular metal–fluorine contacts (A–H) are shown by dashed lines, and intermolecular contacts (I–L) and shown with solid lines.

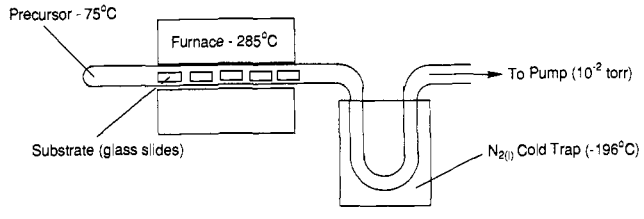

Figure 2. Schematic diagram of the chemical vapor deposition apparatus used in thermal conversion of $(NaOR_f)_4$.

of the Zr atoms were determined from an E-map. The remaining non-hydrogen atoms were obtained from subsequent iterations of least-squares refinement and difference Fourier calculation. The first of the molecules has three well-ordered butoxide ligands and a fourth one (involving C37, C41, and C45) which has an approximate 3-fold disorder about the C–O bond; i.e., it displays three $-CF_3$ groups, each with fluorine atoms at $^2/_3$ occupancy. The second molecule is more badly disordered. In an attempt to account for the electron density which appeared in the difference maps, a total of 63 atoms of varying occupancy were included to represent the 45 atoms of the second molecule. No attempt was made to include the hydrogen atoms. A drawing of the disorder is included as supplementary material. In the final cycles of refinement, the Zr atoms were varied with anisotropic thermal parameters and the other non-hydrogen atoms were varied with isotropic thermal parameters. The largest peak in the final difference map was 2.9 e/Å^3 (located in the second molecule). Although this is somewhat large, the last few changes that had been made to account for the disorder had produced minimal improvement and the work was concluded. The results of the structure determination are shown in Tables I and IV and Figure 3.

X-ray Structure Determination of $Na_2Zr(OCH(CF_3)_2)_6(C_6H_6)_2$. The very air-sensitive well-formed prisms were grown from cooling a saturated solution in C_6H_6. A suitable crystal was affixed to a glass fiber using silicone grease under a nitrogen atmosphere. The goniometer head was then transferred to the goniostat, where the sample was cooled to −172 °C for characterization and data collection.[12] A search of a limited hemisphere of reciprocal space using an automated search routine yielded a set of 24 reflections with monoclinic symmetry and systematic absences corresponding to one of the space groups $C2$, Cm, or $C2/m$. Subsequent solution and refinement confirmed the correct space group to be the centrosymmetric choice, $C2/m$. Data were collected ($6° < 2\theta < 55°$) using standard $\theta/2\theta$ continuous scan techniques with fixed backgrounds at each extreme of the scan. The data were corrected for Lorentz and

Table IV. Selected Bond Distances (Å) and Angles (deg) for "Molecule 2" of $Zr(OCMe(CF_3)_2)_4$ (3)

Zr(1)–O(2)	1.927(11)	Zr(1)–F(28)	3.303(20)
Zr(1)–O(13)	1.906(12)	Zr(1)–F(42)	3.520(20)
Zr(1)–O(24)	1.930(11)	Zr(1)–F(31)	3.739(20)
Zr(1)–O(35)	1.902(13)		
O(2)–Zr(1)–O(13)	107.1(5)	Zr(1)–O(24)–C(25)	153.2(10)
O(2)–Zr(1)–O(24)	110.0(5)	Zr(1)–O(35)–C(36)	165.1(12)
O(2)–Zr(1)–O(35)	111.2(5)	O(2)–C(3)–C(4)	109.1(13)
O(13)–Zr(1)–O(24)	111.0(5)	O(2)–C(3)–C(8)	105.9(13)
O(13)–Zr(1)–O(35)	108.2(5)	O(2)–C(3)–C(12)	112.8(14)
O(24)–Zr(1)–O(35)	109.2(5)	C(4)–C(3)–C(8)	109.4(13)
Zr(1)–O(2)–C(3)	162.3(10)	C(4)–C(3)–C(12)	110.9(13)
Zr(1)–O(13)–C(14)	174.6(10)	C(8)–C(3)–C(12)	108.6(14)

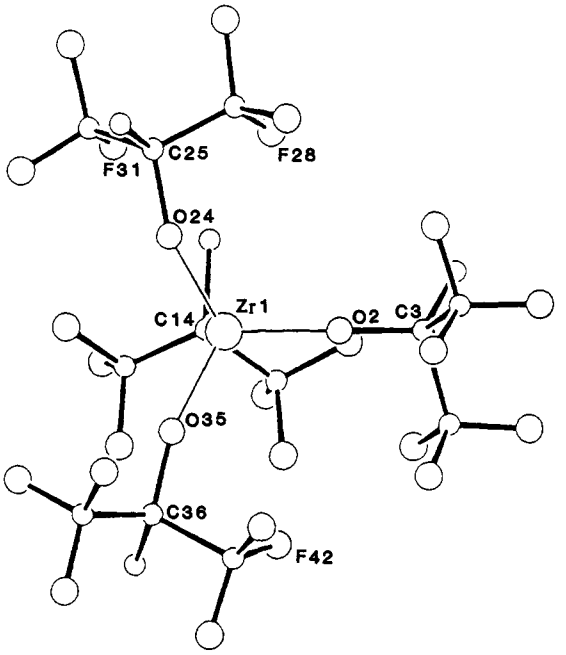

Figure 3. Ball-and-stick drawing of $Zr(OCCH_3(CF_3)_2)_4$ (3), showing selected atom labeling.

Table V. Selected Bond Distances (Å) and Angles (deg) for $Na_2Zr(OCH(CF_3)_2)_6(C_6H_6)_2$ (4b)

Zr(1)–O(2)	2.093(3)	Na(18)–F(9)	2.810(3)
Zr(1)–O(12)	1.998(4)	Na(18)–C(22)	2.966(4)
O(2)–C(3)	1.375(5)	Na(18)–C(21)	2.980(4)
O(12)–C(13)	1.368(7)	Na(18)–C(23)	3.015(4)
C(3)–C(4)	1.530(7)	Na(18)–C(20)	3.139(4)
C(3)–C(8)	1.529(7)	Na(18)–C(24)	3.146(4)
C(13)–C(14)	1.521(6)	Na(18)–C(25)	3.215(4)
Na(18)–O(2)	2.413(4)	Na(18)–C(19)	3.278(4)
Na(18)–O(12)	3.085(4)	Na(18)–C(7)	3.462(3)
Na(18)–F(15)	2.675(3)		
O(2)–Zr(1)–O(2)	180	O(2)–Zr(1)–O(12′)	93.30(13)
O(2)–Zr(1)–O(2′)	94.56(18)	Zr(1)–O(2)–C(3)	135.67(28)
O(2)–Zr(1)–O(2″)	85.44(18)	Zr(1)–O(12)–C(13)	179.7(4)
O(2)–Zr(1)–O(12)	86.70(13)		

polarization terms and averaged to yield a unique set of intensities. Parameters of the unit cell and data collection are shown in Table I. After several attempts to interpret E-maps and Patterson maps, it was realized that the molecule was situated at the origin. Fourier techniques subsequently revealed the rest of the structure, including hydrogen atoms. The benzene molecules have a well-defined disorder, with the two half-weight molecules being rotated 30° with respect to each other. A final difference Fourier was featureless, the largest peak being 0.39 e/Å^3. The results are shown in Tables I and V and Figure 4.

X-ray Structure Determination of $Na_2Zr(OCH(CF_3)_2)_6(C_6H_6)$. Clear, very air-sensitive octahedral crystals were grown from cooling a saturated solution in C_6H_6. A crystal of suitable size was mounted using silicone grease and was transferred to a goniostat, where it was cooled to −170 °C for characterization (Table I) and data collection ($6° < 2\theta < 45°$).[12] A systematic search of a limited hemisphere of reciprocal space yielded a set of reflections which exhibited a rhombohedral-centered hexagonal cell. The cell was indexed as rhombohedral, and subsequent solution and refinement confirmed the space group to be $R\bar{3}$. Data were collected for $\pm h$, $\pm k$, and $+l$. No correction for absorption was performed. The structure was solved by a usual combination of direct methods (MULTAN78) and Fourier techniques. The Zr atom sat at the center of symmetry, resulting in a strong correlation between the Zr thermal parameter and the scale factor. Both independent hydrogen atoms were found in the difference Fourier map. The molecule has a crystallographic 3-fold axis. The results of the structure determination are shown in Tables I and VI and Figure 5.

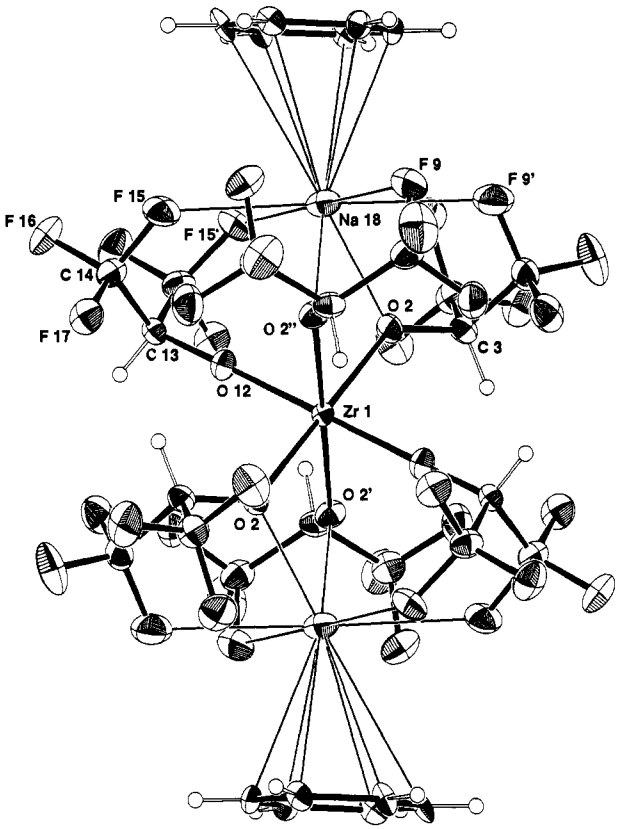

Figure 4. ORTEP drawing of $Na_2Zr(OCH(CF_3)_2)_6(C_6H_6)_2$ (4b), showing selected atom labeling. Thermal ellipsoids are drawn at 50% probability.

Table VI. Selected Bond Distances (Å) and Angles (deg) for $Na_2Zr(OCH(CF_3)_2)_6(C_6H_6)$ (4a)

Zr(1)–O(2)	2.0625(25)	Na–F(7)	2.718(4)
O(2)–C(3)	1.379(4)	Na–F(11)	3.413(3)
C(3)–C(4)	1.521(5)	Na–a	2.815
C(3)–C(5)	1.515(5)	Na–C(13)	3.133(8)
C(13)–C(13′)	1.372(4)	Na–Zr	3.196(2)
Na–O(2)	2.504(4)		
O(2)–Zr(1)–O(2a)	94.62(14)	O(2)–Na–F(7b)	130.4(5)
O(2)–Zr(1)–O(2b)	85.38(14)	O(2)–Na–a	139.8
O(2)–Zr(1)–O(2c)	180.00	F(7)–Na–F(7a)	119.4(5)
Zr(1)–O(2)–C(3)	143.43(23)	F(7)–Na–a	85.7
O(2)–Na–O(2a)	67.9(5)	Zr–Na–O(2)	40.2
O(2)–Na–F(7)	62.8(5)	Zr–Na–F(7)	94.3
O(2)–Na–F(7a)	89.0(5)		

[a] Center of mass of the C_6H_6 ring.

X-ray Structure Determination of $Tl_2Zr(OCH(CF_3)_2)_6$. Colorless, approximately spherical crystals were grown from cooling a saturated solution in C_6F_6. A suitable crystal was mounted using silicone grease and transferred to a goniostat, where it was cooled to −172 °C for characterization (Table I) and data collection ($6° < 2\theta < 45°$).[12] A systematic search of a limited hemisphere of reciprocal space revealed symmetry and systematic absences corresponding to two monoclinic space groups $C2/c$ and Cc. An initial choice of the centrosymmetric one was confirmed by the successful solution of the structure. The structure was

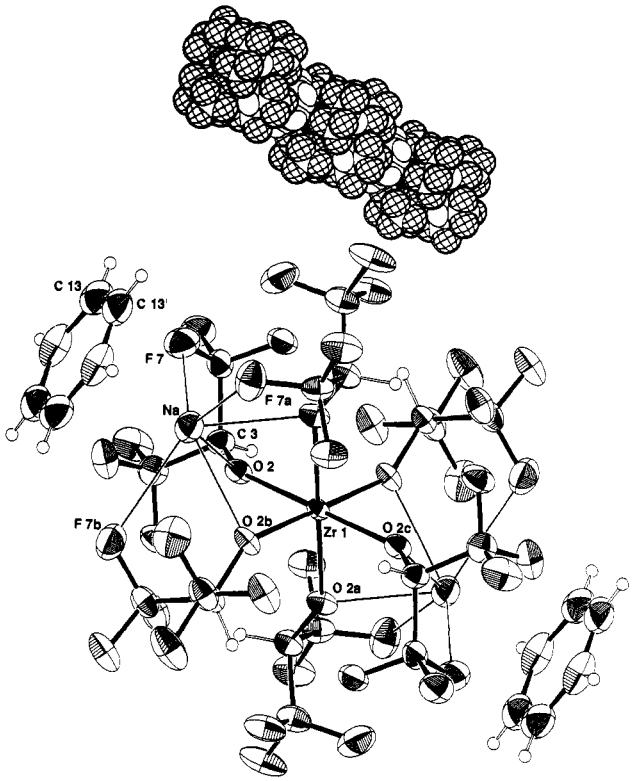

Figure 5. ORTEP drawing of $Na_2Zr(OCH(CF_3)_2)_6(C_6H_6)$ (**4a**), showing selected atom labeling. The second benzene ring is from an adjacent molecule. The space-filling drawing shows the polymeric nature of **4a**. Thermal ellipsoids are drawn at 50% probability, and the space-filling model is drawn at van der Waals radii.

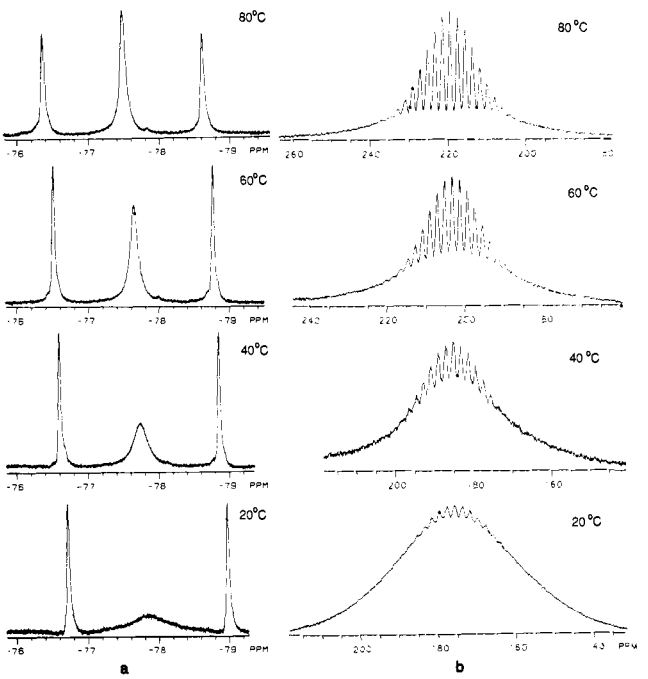

Figure 6. Variable-temperature ^{19}F (a) and ^{205}Tl (b) NMR of $Tl_2Zr(OCH(CF_3)_2)_6$ (**5**) in C_6F_6.

solved by a usual combination of direct methods (MULTAN78) and Fourier techniques. The Tl and Zr positions were obtained from an initial *E*-map, and the remainder of the non-hydrogen atoms were found in subsequent iterations of least-squares refinement and difference Fourier calculations. After partial refinement of the non-hydrogen atoms, hydrogen atoms were included in the calculated positions. The final refinement employed 310 parameters and 2251 reflections. The absorption correction attempts were unsuccessful because of the great number of crystal faces. A final difference Fourier map was essentially featureless,

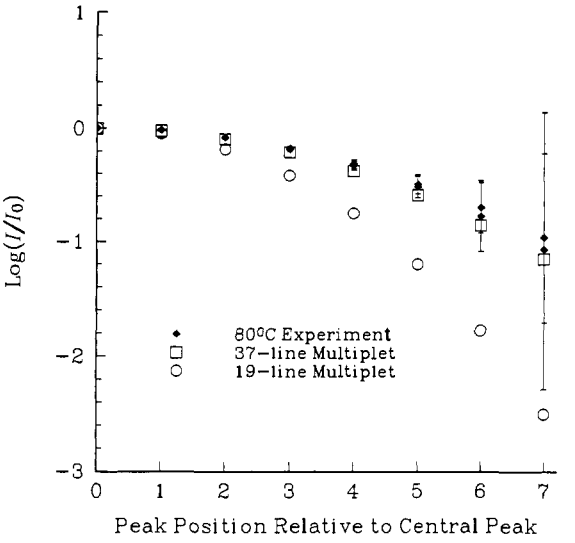

Figure 7. ^{205}Tl NMR transition intensities (and standard deviations) in $Tl_2Zr(OR_f)_6$ at 80 °C. The data is plotted as log (I/I_0) as a function of peak position relative to the central peak (peaks to the left and right of center are plotted together), where I is the intensity of the line and I_0 is the intensity of the central line. Also plotted are theoretical intensities of the same transitions for 19-line multiplets (circles) and 37-line multiplets (squares).

Table VII. Selected Bond Distances (Å) and Angles (deg) for $Tl_2Zr(OCH(CF_3)_2)_6$ (**5**)[a]

Zr(2)–O(21)	2.090(7)	Tl(1)–F(4)	3.135(12)
Zr(2)–O(22)	2.035(8)	Tl(1)–F(6)	3.215(11)
Zr(2)–O(23)	2.054(8)	Tl(1)–F(9)	3.238(11)
O(21)–C(24)	1.373(15)	Tl(1)–F(12)	3.096(8)
O(22)–C(27)	1.409(15)	Tl(1)–F(15)	3.068(8)
O(23)–C(30)	1.384(15)	Tl(1)–F(19)	3.287(11)
C(24)–C(25)	1.550(18)	Tl(1)–F(12)*	3.378(8)
C(24)–C(26)	1.534(18)	Tl(1)–F(19)*	3.442(11)
C(27)–C(28)	1.511(19)	Tl(1)–F(7)**	3.289(11)
C(27)–C(29)	1.539(19)	Tl(1)–O(21)	2.740(9)
C(30)–C(31)	1.532(18)	Tl(1)–O(22)	2.814(10)
C(30)–C(32)	1.523(18)	Tl(1)–O(23)	2.831(11)

O(21)–Zr(2)–O(21′)	180.00	O(22)–Zr(2)–O(23)	94.2(3)
O(21)–Zr(2)–O(22′)	84.8(3)	O(22)–Zr(2)–O(23′)	85.8(3)
O(21)–Zr(2)–O(22)	95.2(3)	Zr(2)–O(21)–C(24)	145.3(8)
O(21)–Zr(2)–O(23′)	94.3(3)	Zr(2)–O(22)–C(27)	146.7(8)
O(21)–Zr(2)–O(23)	85.7(3)	Zr(2)–O(23)–C(30)	148.4(7)

[a] * indicates intermolecular contact to first neighboring molecule; ** indicates intermolecular contact to second neighboring molecule.

except for a few peaks of 3.3–1.2 e/Å^3 in the vicinity of the heavy atoms. Results are shown in Tables I and VII and Figure 8.

Results

$NaOR_f$ (1). (a) Synthesis and Characterization. Investigations into fluoroalkoxides began with the studies of a well-documented system $NaOR_f$[13] (OR_f = hexafluoroisopropoxide). Using a modified synthesis, H–OR_f was deprotonated at room temperature with sodium hydride in diethyl ether (eq 1). Removal of solvent and subsequent recrystallization from toluene produced **1** as colorless rods.

$$NaH + H\text{-}OR_f \xrightarrow{Et_2O} \underset{\mathbf{1}}{NaOR_f} + H_2 \qquad (1)$$

The compound is soluble in ethers and hexafluorobenzene but has low solubility in aromatic solvents. Its physical characteristics, such as melting point (120 °C) and sublimation conditions (75

(13) (a) Kioetzsch, H. J. *Chem. Ber.* **1966**, *99*, 1143. (b) Dear, R. E. A.; Fox, W. B.; Fredericks, R. J.; Gilbert, E. E.; Huggins, D. K. *Inorg. Chem.* **1970**, *9*, 2590.

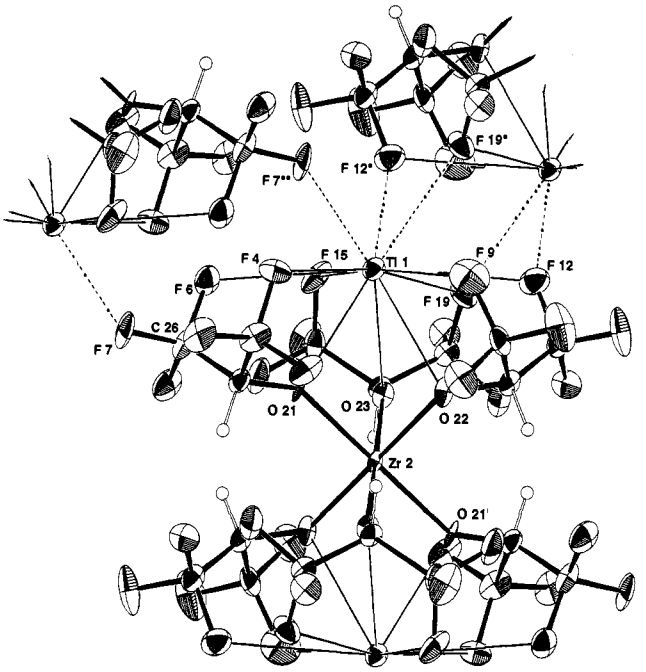

Figure 8. ORTEP drawing of $Tl_2Zr(OCH(CF_3)_2)_6$ (**5**) and portions of the two nearest neighboring molecules, showing selected atom labeling. Intermolecular contacts are represented by dashed lines. Thermal ellipsoids are drawn at 50% probability.

°C at 10^{-2} Torr), are consistent with previous reports. It is also found to sublime at 140 °C at 1 atm of helium. The volatility of $NaOR_f$ is significantly greater than its hydrocarbon analogue (190 °C at 10^{-2} Torr with some decomposition).

The ^{19}F NMR spectrum of **1** in either C_6F_6 or d_8-toluene exhibits one doublet at −83.4 or −79.8 ppm (J_{H-F} = 6.5 Hz), respectively. The large difference of chemical shifts is due to the strong solvent dependence inherent to ^{19}F NMR.[14] The proton NMR spectrum shows a single septet at 4.35 ppm in C_6F_6 and 4.12 ppm in d_8-toluene. This spectroscopic information indicates that the fluoroalkoxides are equivalent on the NMR time scale either by some fluxional process or by oligomerization to a symmetrical structure. Literature reports did not ascertain the degree of oligomerization due to the limited solubility in noncoordinating solvents. However, given the simplicity of these spectra and the universal tendency of $(M^1OR)_n$ compounds to aggregate (n = 2–∞), we determined the structure of solid $NaOR_f$.

(b) Solid-State Structure. X-ray quality crystals of the empirical formula $NaOCH(CF_3)_2$ were grown via slow sublimation in sealed tubes, producing clear colorless plates. Diffraction of these crystals established that the molecule is a tetramer in the slightly distorted cubane configuration shown in Figure 1. The metal–oxygen distances range from 2.250(4) to 2.342(5) Å, and the O–Na–O angles are 88.11(8)–91.54(8)°; these variations represent some 30 esd's. Angles within the $CH(CF_3)_2$ group are unexceptional, but the Na–O–C angles span a wide range: 115.8(2)°–137.4(2)°. Such variable bending occurs in order to increase the coordination environment of sodium from trigonal pyramidal (i.e., NaO_3) to NaO_3F_n by virtue of F→Na bonds both within cubes (A–H in Table II and represented by dashed lines in Figure 1) and between cubes (Table III and lines I–L in Figure 1). The latter connect the solid into an infinite three-dimensional polymer. These intermolecular bond lengths are variable, with that to Na(4) being particularly weak. Intramolecular F→Na bonds shorter than the combined van der Waals radii are included in Table II. This reveals that Na(4), with the weakest intermolecular F→Na bond, compensates by having the most (i.e., three) intramolecular bonds to fluorine. With the exception of Na(4), the intermolecular Na–F distances are shorter than the intramolecular ones. This is likely to be a conformational effect, since the fluorines are directed away from the metal–oxygen core and can more readily coordinate to a metal center of an adjacent molecule than bend upon itself to coordinated intramolecularly. Organofluorine donation to Na^+ causes no significant lengthening of C–F bonds.

It should be noted that, while the number of sodium–fluorine interactions vary, the average sodium–oxygen distances remains relatively constant (i.e., the sodium with the largest number of closest fluorine contacts does not have the longest sodium–oxygen distances). This may indicate that the Na–F contacts have a large electrostatic component (see later).

It was not possible to uniquely identify Na–F interactions via IR spectroscopy because metal–oxygen bonds of the alkoxides obscure the region in which metal–fluorine interactions would be observed. The C–F stretching region was also investigated for indications of metal–fluorine interactions (bands of lower vibrational energy), but no definitive assignments could be made.

(c) CVD of 1. In order to observe the effects of fluorination of alkoxides on the deposition of inorganic material, a CVD study was performed on **1**. The all-glass apparatus (Figure 2) consisted of an independently heated source chamber, a hot-walled reactor containing glass plate substrates where deposition takes place, and a liquid nitrogen trap downstream from the reactor to collect the volatile products. The overall system was evacuated to 10^{-2} Torr. Sublimation at 75 °C transported **1** into the reactor, which was heated to 285 °C. Over a course of 6 h, an off-white iridescent coating was deposited on the reactor walls and the glass substrates. At temperatures greater than 295 °C, the coatings were significantly darker, indicative of a high carbon content. At lower temperatures (<260 °C), deposition was incomplete, with a major amount of precursor passing through the reactor unchanged.

Analysis of the deposited solid by powder X-ray diffraction revealed that the crystalline material was sodium fluoride (NaF). Bulk elemental analysis of the solid confirmed this result, with the sample consisting of >98% NaF (0.5% C).

The volatiles from the deposition reaction were isolated downstream of the reactor in two phases, a viscous amber oil just outside of the hot zone and a colorless liquid in the liquid nitrogen trap. The viscous oil was found to be insoluble in aromatic solvents. Fluorinated solvents were avoided due to potential interference with NMR analysis. However, the oil was completely soluble in d_8-THF. The ^{19}F NMR spectrum indicates that the oil is a mixture of products containing (ca. 5%) unreacted **1**. The other components of the mixture produce broad signals: −65.2 and −66.7 ppm (360-Hz half-height, ca. 10% each), −74.5 and −75.0 ppm (210-Hz half-height, ca. 30% and 50%, respectively) in the region of aliphatic $-CF_3$ groups, and −225.1 ppm (600-Hz half-height, ca. 5%) falling in the region for fluorine attached to olefinic carbons.

The ^1H NMR spectrum of the oil indicates similar patterns. The signals for **1** and major products at 6.4 and 5.5 ppm (also very broad and ca. 30% and 50%, respectively) are resolved. These signals are consistent with highly deshielded protons, possibly due to fluorine inductive effects. Minor products are observed at 6.8 and 6.7 ppm (ca. 5% each). This is evidence of some vinylic material being present based on both the proton and fluorine spectral data, but this material is only a minor component (ca. 10% total). Given the limited fine structure of both spectra, little can be concluded about the major products except that the broad nature of the signals as well as the oily physical appearance of the material suggests a polymeric material with both fluorine- and proton-containing units.

The contents of the liquid nitrogen trap were vacuum transferred to an NMR tube containing C_6D_6. The ^{19}F NMR spectrum indicates that the main product is hexafluoroisopropyl alcohol (ca. 70%). The other 30% is made up of at least nine

(14) Emsley, J. W.; Phillips, L. *Prog. NMR Spectrosc.* **1971**, *7*, 1.

other trace signals appearing as doublets. The proton NMR spectrum confirms that the alcohol is the major product among a variety of other complex signals ranging from 5.5 to –0.1 ppm.

$Zr(OCH(CF_3)_2)_4$ (2). The compounds ZrX_4 generally aggregate by X-bridging. Given the surprising degree of organofluorine-to-sodium interaction in $NaOCH(CF_3)_2$, we therefore turned our attention to $Zr(OCH(CF_3)_2)_4$. This compound was synthesized previously[15] from $ZrCl_4$ and $NaOR_f$ in neat R_fOH. In an attempt at simplification (and avoidance of possible solvent coordination in the product prior to sublimation), we reacted $ZrCl_4$ with 4 quiv of $NaOR_f$ in refluxing benzene. This, however, gave $Na_2Zr(OR_f)_6(C_6H_6)_n$ (eq 2a). Attempts at alcoholysis or alcohol exchange also failed to give simply $Zr(OR_f)_4$ (eq 2b).[16]

$$ZrCl_4 + 4NaOR_f \xrightarrow[\Delta]{C_6H_6} Na_2Zr(OR_f)_6 \qquad (2a)$$

$$(ZrX_4)_n + \text{excess } R_fOH \xrightarrow{C_6H_6} ZrX_{4-n}(OR_f)_n(HX) \qquad (2b)$$

$$x = NMe_2, O^tBu, O^iPr;\ n = 3, 4$$

Complete substitution was not possible even with refluxing the reaction in the fluorinated alcohol or repeated azeotropic distillations in benzene or toluene. Alcoholysis of tetraneopentylzirconium (eq 2c), however, gave the desired product as colorless

$$Zr(CH_2CMe_3)_4 + \text{excess } R_fOH \xrightarrow{C_6H_6} \underset{\mathbf{2}}{Zr(OR_f)_4} + 4CMe_4 \qquad (2c)$$

crystals which could be purified by recrystallization from hot benzene or sublimed under very mild conditions (60 °C, 10^{-2} Torr). **2** will also sublime at 77 °C at 1 atm of helium. **2** is found to be extremely reactive with moist air, quickly liquefying to an oil. The zirconium compound has poor solubility in aromatic and aliphatic solvents but is very soluble in hexafluorobenzene.

The ^1H NMR spectrum of **2** in hexafluorobenzene shows a broad septet at 4.79 ppm (J = 5.4 Hz), and the ^{19}F NMR spectrum shows a very broad singlet at –77.3 ppm ($\Delta\nu_{1/2}$ = 260 Hz). A variety of fluxional processes could account for the broadness of the signal. Association/dissociation of zirconium fluoroalkoxide units bridged by either oxygen (i.e., $(Zr(OR_f)_4)_x$)[17] or fluorine (i.e., $(NaOR_f)_4$) is possible. Alternatively, intramolecular interaction of γ-fluorines with the metal center also would produce broadening of the NMR signal via restricting the rotation of the $-CF_3$ groups about the carbon–carbon single bond.

It was not possible to grow crystals suitable for X-ray structural determination by either slow sublimation or slow cooling of saturated solutions in benzene or toluene due to twinning problems.

$Zr(OCMe(CF_3)_2)_4$ (3). (a) Synthesis and Characterization. In an attempt to gain some crystallographic information about homometallic zirconium fluoroalkoxides, the analogous species $Zr(OCCH_3(CF_3)_2)_4$ ($Zr(OR_f')_4$) was investigated. It was anticipated that the steric profile of this alkoxide would perturb the system sufficiently to prevent the twinning problems previously encountered.

Compound **3** was synthesized from tetraneopentylzirconium and hexafluoro-*tert*-butyl alcohol in a reaction similar to that of eq 2c. The resulting $Zr(OR_f')_4$ was significantly more soluble in hydrocarbon solvents than the OR_f derivative, and its volatility was also found to have increased (sublimed at 35 °C and 10^{-2} Torr).

The ^1H and ^{19}F NMR spectra of **3** in C_6F_6 show none of the broadness found for **2**. The signals are sharp singlets at 1.55 and –82.9 ppm, respectively. This is likely the result of the increased bulk at the zirconium which may prevent the association of γ-fluorines to the metal center.

(b) Solid-State Structure. X-ray quality crystals of the empirical formula $Zr(OCCH_3(CF_3)_2)_4$ were grown via slow sublimation in sealed tubes producing clear colorless prismatic plates. Diffraction of these crystals established the molecule to be a monomer (Figure 3) based on a ZrO_4 tetrahedron with O–Zr–O angles ranging from 107.1(5) to 111.2(5)° (Table IV). Metal–oxygen distances were found to range from 1.902(15) to 1.930(11) Å, nearly identical to terminal zirconium–oxygen distances in the non-fluorinated compound $Zr_2(O^iPr)_8(HO^iPr)_2$[18] (1.943(5) Å average), even though the latter has a higher metal coordination number. The closest fluorine approach to zirconium is 3.303(20) Å, over 0.6 Å longer than the shortest intramolecular M–F contact in **1**. This poor interaction with the coordinatively unsaturated metal center can be attributed to steric constraints which may prevent the fluoroalkoxides from bending toward the metal, giving rise to intramolecular fluorine interactions. Steric crowding is also likely the main effect preventing the association of molecular units. In addition to the steric influence of the ligands, the very obtuse Zr–O–C angle (153.2(10)–174.6(10)°) is consistent with either π donation from the alkoxide oxygen lone pairs to the metal center or the highly ionic alkoxy oxygen behaving as an isotropic point charge.[19]

$Na_2Zr(OCH(CF_3)_2)_6$ (4). (a) Synthesis and Characterization. The species $Na_2Zr(OR_f)_6$ was initially precipitated when attempting to synthesize $Zr(OR_f)_4$ from $ZrCl_4$ and $NaOR_f$ in benzene. After the reaction stoichiometry was adjusted to reflect that of the final product (i.e., 1:6), **4** could be sublimed from the reaction mixture in moderate yield (50%) (eq 3a). Alternatively,

$$ZrCl_4 + 6NaOR_f \xrightarrow[\Delta]{\text{toluene}} \underset{\mathbf{4}}{Na_2Zr(OR_f)_6} + 4NaCl \qquad (3a)$$

because of the Lewis acidity of **2**, the complexation of zirconium fluoroalkoxide with 2 equiv of $NaOR_f$ in benzene gives $Na_2Zr(OR_f)_6(C_6H_6)_n$ in quantitative yield (eq 3b). Recrystallized

$$Zr(OR_f)_4 + 2NaOR_f \xrightarrow[\Delta]{C_6H_6} \underset{\substack{\mathbf{4a,b}\\ n = 1, 2}}{Na_2Zr(OR_f)_6(C_6H_6)_n} \qquad (3b)$$

solid **4**, isolated from benzene, was found to contain solvent (by NMR) and yielded the general formula $Na_2Zr(OR_f)_6(C_6H_6)_n$ (n = 1 (**4a**), 2 (**4b**)). A mixture of clear colorless octahedra (**4a**) and prisms (**4b**) was obtained. Benzene content was established by X-ray diffraction. The benzene is lost under vacuum or gaseous nitrogen purge (3–5 h), on the basis of the lack of C_6H_6 signals in the proton NMR of evacuated **4a,b** with C_6F_6 as a solvent. The molecule was found to also coordinate tetrahydrofuran by NMR, but sublimation is required to remove this ligand. Compound **4** is only slightly soluble in aromatic solvents but dissolves readily in C_6F_6. This heterometallic compound sublimes at 110 °C and 10^{-2} Torr or at 145 °C and 1 atm of helium without residue.

The ^{19}F NMR spectrum of **4** in C_6F_6 shows a broad doublet at –80.5 ppm (J_{H-F} = 3.4 Hz); in C_6D_6, the chemical shift is at –78.0 ppm. The large difference is due to the general solvent-dependence of fluorine chemical shifts.[14] The proton NMR spectrum in C_6F_6 shows a poorly-resolved (broad) septet at 4.63 ppm. Compound **4** appears relatively inert to $NaOR_f$ exchange.

(15) Mazdiyasni, K. S.; Schaper, B. J.; Brown, L. M. *Inorg. Chem.* **1971**, *10*, 889.
(16) Products analyzed by NMR.
(17) Bradley, D. C.; Mehrotra, R. C.; Goen, P. D. In *Metal Alkoxides*; Academic Press: London, New Yor, San Francisco, 1978; Chapter 3.
(18) Vaartstra, B. A.; Huffman, J. C.; Gradeff, P. S.; Hubert-Pfalzgraf, L. G.; Daran, J.-C.; Parraud, S.; Yunlu, K.; Caulton, K. G. *Inorg. Chem.* **1990**, *29*, 3126.
(19) Cayton, R. H.; Chisholm, M. H.; Davidson, E. R.; DiStasi, V. F.; Du, P.; Huffman, J. C. *Inorg. Chem.* **1991**, *30*, 1020.

A mixture of $Na_2Zr(OR_f)_6$ and $NaOR_f$ in C_6F_6 shows no line broadening or change in chemical shift of the species present. Thus, any exchange of $-OR_f$ is slow if it occurs at all. Since the molecular unit $Na_2Zr(OR_f)_6$ appears to stay intact in nonpolar solvent, and there is no single geometry that would have all the trifluoromethyl groups equivalent, we conclude that there is rapid rotation around the C–C and C–O bonds of the alkoxides. This would result in a single time-averaged signal on the NMR time scale. The broadness of the ^{19}F NMR signal can be attributed to two sources. The first is restricted rotation around the single bonds from a combination of steric congestion and coordination to the sodium center. The second source could be quadrupolar coupling from the sodium center, broadening the NMR signal. This broadening of fluorine signals by quadrupoles has been observed before.[20] The proton NMR of either benzene adduct (**4a,b**) in C_6F_6 shows a peak at the chemical shift of free benzene. This ready dissociation may indicate that the benzene merely resides in the lattice and does not interact with the sodium. A second, more likely explanation is that the benzene is displaced by hexafluorobenzene. The coordinated fluorobenzene would then be in rapid exchange with the bulk of the solvent.

(b) Solid-State Structures. Upon very slow cooling of a benzene solution of **4**, two morphologies of colorless crystals were produced (**4a,b**). The solid-state structure of **4b** with empirical formula $Na_2Zr(OCH(CF_3)_2)_6(C_6H_6)_2$ (Figure 4 and Table V) reveals a $Na(\mu\text{-}OR_f)_2Zr(OR_f)_2(\mu\text{-}OR_f)_2Na$ structural unit centered around a ZrO_6 octahedron with two terminal, linear ($\angle$Zr–O–C = 179.7(4)°) alkoxides and four bridging, bent ($\angle$Zr–O–C = 135.7(3)°) alkoxides. The linear alkoxides bond more strongly to zirconium than do the bent ones (Zr–O = 1.998(4) and 2.093(3) Å, respectively). Sodium is equidistant from the two O(2) donors (2.413(4) Å), but is nonbonding to the linear O(12) (Na(18)–O(12) = 3.085(4) Å). This bent two-coordinate environment of sodium is supplemented by bonding to four fluorines at Na–F distances of 2.673(3) Å (twice) and 2.810(3) Å (twice). This *planar* NaF_4 substructure of each sodium is complemented by the π-cloud of a benzene ring. These benzenes were found to have a well-defined crystallographic disorder, with two statistically equally weighted molecules rotated 30° with respect to each other. The first configuration has the mirror plane of the heterometallic alkoxide passing between the carbons of the ring (C(19)–C(21)) with two carbons close to sodium (Na–C(21) = 2.980(4) Å) and four more distant (3.139(4) and 2.980(4) Å, each twice). The second position has the mirror plane of the molecule bisecting two of the carbons of the benzene (C(22)–C(25)) with one carbon being closest to the sodium (Na–C(22) = 2.966(4) Å) and one carbon being most distant on the other side of the ring (Na–C(25) = 3.215(4) Å).

In contrast, **4a** with empirical formula $Na_2Zr(OCH(CF_3)_2)_6(C_6H_6)$ adopts a solid-state structure (Figure 5 and Table VI) with an infinite chain of alternating benzene and $Na_2Zr(OCH(CF_3)_2)_6$ links. Each of these units lies around a C_3 axis with centers of symmetry at Zr and at the center of the benzene ring. This means that all alkoxide groups are equivalent and bent ($\angle$Zr–O–C = 143.4(2)°). Every Na forms three identical (Na–O = 2.50 Å) bonds to oxygen and three Na–F bonds (2.72 Å). Benzene is bound equally to two centrosymmetrically-related sodiums with an Na–C distance of 3.13 Å. The six identical Zr–O distances are 2.063(3) Å.

That both compositions of matter (**4a,b**) adopt structures with sodium(1+)–benzene bonding and that a change in benzene content alters the F and O composition of the sodium coordination sphere show the effect of such interactions and their contribution to the lattice energy. Sodium–aromatic interactions with "long" carbon–metal distances are precedented in sodium tetraphenyl allyl etherate in which sodium has been shown to bind exclusively to the phenyl rings at distances ranging from 2.720(8) to 3.100(8) Å.[21] Sodium–mesitylene interactions also have been observed in $(C_6H_3Me_3)_2Na_4(HBEt_3)_4$ with Na–C distances ranging from 2.85 to 3.05 Å.[22] For $Na_2Zr(OR_f)_6(C_6H_6)_n$, alternative structures with benzene elsewhere in the lattice would involve destabilizing π-cloud–fluorine repulsions.

$Tl_2Zr(OCH(CF_3)_2)_6$ (5). (a) Synthesis and Characterization. In order to investigate the metal–fluorine interactions in solution, as well as in the solid state, Tl^+ was used in place of Na^+. This replacement[23] was made because thallium is a convenient NMR probe (^{205}Tl has spin $I = {}^1/_2$, is 70.48% abundant, and has a gyromagnetic ratio of 24.57 MHz/T). In addition, thallium(1+) is a much "softer" ion than sodium, hence providing the opportunity to observe how fluorine, a "hard" center, interacts with such metals.

The synthesis of **5** was analogous to that of **4** in refluxing benzene or toluene, producing a white microcrystalline solid (eq 4).

$$Zr(OR_f)_4 + 2TlOR_f \xrightarrow[\Delta]{C_6H_6} \underset{\mathbf{5}}{Tl_2Zr(OR_f)_6} \qquad (4)$$

This material is only slightly soluble in boiling benzene and has a low solubility in C_6F_6. **4** is found to weakly coordinate THF, which can be readily removed *in vacuo*. The thallium complex has volatility similar to the sodium analogue, subliming at 120 °C at 10^{-2} Torr.

Spectroscopic characterization of **5** in hydrocarbon solvents proved impossible due to poor solubility. The room-temperature ^1H NMR spectrum in C_6F_6 reveals a single signal at 4.90 ppm, a broad septet with poorly-resolved fine structure. At elevated temperature, the signal sharpens slightly, taking on more septet characteristics. The ^{19}F NMR spectrum at 20 °C (Figure 6a) appears as two sharp peaks separated by 765 Hz, centered around a broad ($\Delta\nu_{1/2}$ = 229 Hz) feature at −77.8 ppm in an approximate integral ratio of 1:2:1 (F–H coupling of less than 5 Hz is not resolved). This splitting is independent of spectrometer field strength (340 *vs* 283 MHz), indicating splitting is a result of Tl–F coupling rather than two chemical shifts. The above spectra are best interpreted in terms of a fluxional process making all fluorines equivalent.

Variable-temperature spectra (Figure 6a) reveal that by +80 °C,[24] the signal resolves to an apparent triplet with J = 383 Hz, which we suggest is due to coupling to two thallium centers. Evidence for the fluxionality required by this interpretation is obtained from dynamic NMR measurements. We find that the fluorine T_1 (from inversion–recovery experiments) is long (~1 s) and relatively insensitive to temperature (over the range studied), while the fluorine T_2 (from spin–echo experiments) matches the inverse line width, and this is quite temperature-dependent and substantially smaller than T_1. Therefore, there exists an efficient dephasing mechanism that is separate from the population relaxation, as is typical of fluxional molecules. The dramatic temperature-dependence of the line width and the relaxation data indicate that $Tl_2Zr(OR_f)_6$ is a dynamic molecule:[25] in contrast to the ground-state structure, with chemically-inequivalent fluorines of the trifluoromethyl groups, intramolecular rearrangement causes time-average equivalence of all 36 fluorines and each fluorine is visited by *both* thallium centers during the fluxional process. We sought to confirm these

(20) (a) Jorris, T. L.; Kozik, M.; Baker, L. C. W. *Inorg. Chem.* **1990**, *29*, 4584. (b) Boyd, A. S. F.; Davidson, J. L.; McIntosh, C. H.; Leverd, P. C.; Lindell, W. B.; Simpson, N. J. *J. Chem. Soc., Dalton Trans.* **1992**, 2531.

(21) Bock, H.; Ruppert, K.; Havlas, Z.; Fenske, D. *Angew. Chem., Int. Ed. Engl.* **1990**, *29*, 1042.

(22) Köster, R.; Schüble, W.; Boese, R.; Bläser, D. *Chem. Ber.* **1991**, *124*, 2259.

(23) Samuels, J. A.; Zwanziger, J. W.; Lobkovsky, E. B.; Caulton, K. G. *Inorg. Chem.* **1992**, *31*, 4046. ^{203}Tl ($I = {}^1/_2$) is 29.52% abundant.

(24) Low-temperature spectra are precluded because of the freezing of C_6F_6.

(25) Pople, J. A.; Schneider, W. G.; Bernstein, H. J. In *High-Resolution Nuclear Magnetic Resonance*; McGraw-Hill: New York, 1959; Chapter 10.

Scheme I

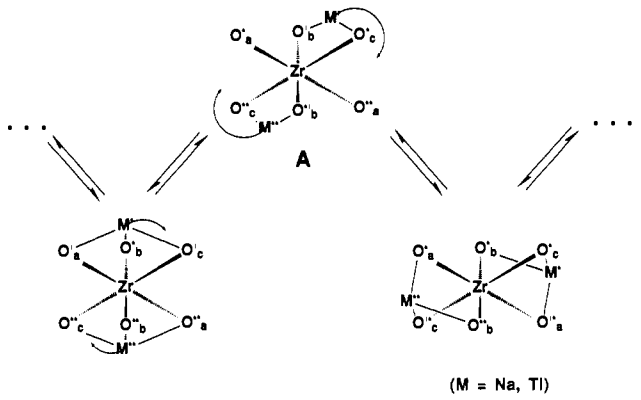

conclusions by recording the ^{205}Tl NMR spectrum at various temperatures (Figure 6b). In C_6F_6 at 21 °C, a broad ($\Delta\nu_{1/2}$ = 3700 Hz) resonance is observed, with ca. seven lines (spacing 383 ± 14 Hz) resolved at the center of the pattern. At +40 °C, +60 °C, and +80 °C, these lines sharpen (J_{Tl-F} = 388 ± 12.7 Hz) and at least 19 lines are resolved. The falloff of the intensities of these 19 lines (Figure 7) fits well with that predicted for the centermost lines of a binomial distribution for 36 spin-$^1/_2$ particles and is inconsistent with the corresponding calculation for 18 spin-$^1/_2$ particles. The difference between the two patterns is distinctive: for example, in a 19-line multiplet, the peaks removed by five from the central line are 6.3% as intense as the central line, while in the 37-line pattern they are 25% as intense, and in our data, 30% as intense. The outermost lines in the spectrum provide another qualitative check: in a 19-line pattern, these are five orders of magnitude less intense than the central line, so the pattern we observe cannot be due to interaction with only 18 fluorines (in a 37-line multiplet, the outer lines are down by 10 orders of magnitude, so of course we cannot observe them). The Tl NMR results thus provide independent evidence that there is global intramolecular migration of the two Tl centers over all eight ZrO_3 triangular faces within the molecule $Tl_2Zr(OR_f)_6$.[28]

Scheme I portrays a mechanism of thallium migration passing through a $Zr(\mu\text{-}OR_f)_2Tl$ transition state with the $Zr(OR_f)_6$ octahedron held rigid. This rearrangement, together with Tl–F bond rupture/reformation and rapid rotation about C–CF_3 bonds, is sufficient to explain the full set of spectral observations.[26,27]

(b) Solid-State Structure. A sample of **5** was recrystallized from hexafluorobenzene as clear, colorless, nearly-spherical crystals. Unlike the sodium system, the thallium species is solvent-free with the empirical formula $Tl_2Zr(OCH(CF_3)_2)_6$ (Figure 8 and Table VII). The structure is centrosymmetric, containing a crystallographic inversion center lying at the zirconium atom. The zirconium center is surrounded by six fluoroalkoxides in a slightly distorted octahedron, capped on *trans* faces by thallium ions giving the overall molecular unit $Tl(\mu_2\text{-}OR_f)_3Zr(\mu_2\text{-}OR_f)_3Tl$. The zirconium–oxygen distances are 2.090(7) (O(21)), 2.035(8) (O(22)), and 2.054(8) Å (O(23)), nearly identical to those found in **4a**. The O–Zr–O angles of the face of the zirconium–oxygen octahedron which contains the thallium are smaller than those without the ion (85.4° *vs* 94.5° average). This is due to the attractive forces of the heteroatom on the three oxygens of the face of the octahedra, giving an elongated appearance to the octahedron.

The oxygen–thallium distances are 2.740(9) (O(21)), 2.814(10) (O(22)), and 2.831(11) Å (O(23)), giving the thallium a coordination number of three with respect to oxygen. The coordination at thallium is increased by intramolecular interactions with γ-fluorines similar to those observed in **1** and **4a,b**. In **5**, there are six contacts around the equator of the thallium ion with distances ranging from 3.068(8) to 3.287(11) Å. These distances are of similar magnitude to those found in TlF, but shorter than in "salts" of thallium cations containing fluorinated anions.[29-31] One fluorine is donated from each trifluoromethyl group of the three alkoxides per face of the octahedron. This is accomplished by directing every isopropyl hydrogen *anti* to Tl. Since all six fluorine contacts are essentially coplanar, the coordination environment of the thallium at this point fills only one hemisphere, leaving the other relatively exposed. In fact, the unit $Tl_2Zr(OR_f)_6$ is actually the repeat unit of a polymeric solid where each thallium ion interacts with fluorines from two neighboring molecules. The intermolecular interactions with the first neighbor are accomplished by the close approach of two fluorines ($F(19)^*_{inter}$ = 3.442(11) Å, $F(12)^*_{inter}$ = 3.378(8) Å) which are already involved in intramolecular Tl–F contacts. The bridge to the second neighbor molecule is via a fluorine which is directed radially (i.e., outward from the noncrystallographic C_3 axis of the $Tl_2Zr(OR_f)_6$ molecule) and which has no other short contacts to a metal ($F(7)^*_{inter}$ = 3.289(11) Å). These interactions produce a two-dimensional lattice in the solid state. However, as indicated by the previously-described NMR data, this extended lattice is not retained in solution. The combination of intra- and intermolecular contacts produces a 12-coordinate thallium ion in the solid state. Since all the ligands to the thallium are roughly distributed evenly around the metal center, it can be concluded that the lone pair of thallium(I) is not stereochemically active in the solid-state structure of **5**. This is fairly common for 6th row main group elements where the "6s" orbital is very diffuse.[32]

Mass Spectrometric Analysis. Mass spectra were obtained on species **1**, **2**, **4**, and **5** in order to gain information on the degree of oligomerization of the species in the gas phase, possible mechanisms of decomposition, and evidence of retention of M–F contacts. Samples were sublimed into the mass spectrometer, where they were ionized via electron bombardment, usually at 15–30 eV. The results are recorded as supplementary material.

The mass spectrum of **1** at 15 eV revealed the most stable ionized forms were the products of the elimination of anions from the tetramer. No parent ion was detected. The highest mass of significant population observed was $[Na_4(OR_f)_3]^+$, the product of the expulsion of OR_f^- from **1**. Elimination of larger anionic clusters was also apparent given the presence of $[Na_3(OR_f)_2]^+$ and $[Na_2OR_f]^+$. It is important to note that metal fluorines were observed in appreciable amounts as $[Na_4F(OR_f)_2]^+$, $[Na_3F_2]^+$, and $[Na_2F]^+$. This implies that metal–fluoride contacts are retained in the gas phase such that when the C–F bond is cleaved, the resulting fluoride is retained in the cluster. Numerous metal-free ions were also observed. At higher sample temperatures, more complex cationic species such as $[Na_6F(OR_f)_4]^+$ and $[Na_5$-

(26) The *J* observed here is time-averaged over instantaneous structures with six "close" $^1J_{Tl-F}$ and 30 "distant" J'_{Tl-F}. Taking the latter to be near zero, the $^1J_{Tl-F}$ for the close contacts can be estimated to be 2298 Hz. This is to be compared to the Tl coupling to an ortho fluorine in $CpMo(SC_6F_5)_4Tl$ of 3630 Hz: Wan Abu Bukar, W. A.; Davidson, J. L.; Lindsell, W. E.; McCullough, K. J.; Muir, K. W. *J. Chem. Soc., Dalton Trans.* **1989**, 991.

(27) The retention of two sharp lines even at dynamic exchange rates which broaden other lines of the spectrum is a consequence of $|\beta\beta\rangle$ becoming $|\beta\beta\rangle$ after a thallium "hop" and likewise $|\alpha\alpha\rangle$ becoming $|\alpha\alpha\rangle$, in contrast to the relatively efficient $|\alpha\beta\rangle \leftrightarrow |\beta\alpha\rangle$ interconversion. For another example (in *cis*-$H_2Fe[P(OEt)_3]_4$), see: *Transition Metal Hydrides*; Muetterties, E. L., Ed.; Marcel Dekker: New York, 1971; pp 181–187.

(28) A second fluxional mechanism involving the formation of $(Tl_2Zr(OR_f)_6)_n$ aggregates was rejected on the basis of retention of Tl–F coupling at elevated temperatures, conditions which should reduce aggregation.

(29) Noirot, M. D.; Anderson, O. P.; Strauss, S. H. *Inorg. Chem.* **1987**, *26*, 2216.

(30) Wieghardt, K.; Kleine-Boymann, M.; Nuber, B.; Weiss, J. *Inorg. Chem.* **1986**, *25*, 1309.

(31) Interatomic distances for thallium fluoride: two short (2.25–2.62 Å), two intermediate (2.66–2.79 Å), and two long (3.07–3.90 Å). See: Alcock, N. W.; Jenkins, H. D. B. *J. Chem. Soc., Dalton Trans.* **1974**, 1907.

(32) Huheey, J. E. *Inorganic Chemistry*, 3rd ed.; Harper and Row: New York, 1983; Chapters 5 and 15.

$(OR_f)_4]^+$ were detected. An increase of ionization energy from 15–30 eV resulted in no significant change in the mass spectral pattern.

An examination of **2** at 15 eV did reveal a parent ion peak of 758 amu, which would indicate that the homometallic zirconium fluoroalkoxide ion has greater stability than **1**, **4**, and **5**. Other ions were detected including $[Zr(OR_f)_3]^+$, $[ZrF(OR_f)_2]^+$, and $[ZrF_2OR_f]^+$. This indicates that **2** undergoes decomposition similar to that of **1** in that complete OR_f groups are eliminated and metal–fluoride bonds are formed. Unlike the other fluoroalkoxides reported here, **2** shows numerous other metal-containing ions which correspond to more complex fragmentation of the ligands. Whether those other ions lie on the mechanistic pathway to the above zirconium alkoxy fluorides is not known. As with **1**, the mass spectrum of **2** also shows extensive formation of fluorocarbon ions. An increase of ionization energy from 15–30 eV results in a decrease in the yield of heavy and intermediate mass peaks and an increase of metal-free fragment ions.

For the mixed-metal complexes **4** and **5**, the mass spectra were similar to that of **1** in that, at 30 eV, no parent ion peak was detected and the main form of fragmentation is the loss of anionic units. This produced species such as $[M^1_2Zr(OR_f)_5]^+$, $[M^1Zr(OR_f)_4]^+$, and $[M^1_2OR_f]^+$ (M^1 = Na, Tl). Also present were metal fluorides in the forms $[M^1_2ZrF(OR_f)_4]^+$, $[M^1_2ZrF_2(OR_f)_3]^+$, and $[M^1_2F]^+$. Unlike the mass spectra of **1**, **4** and **5** did produce significant amounts of higher molecular weight species $[M^1_3ZrF(OR_f)_5]^+$, $[M^1_3ZrF_2(OR_f)_4]^+$, $[Na_3Zr(OR_f)_6]^+$, and $[Na_4Zr(OR_f)_7]^+$ at all sample temperatures. This information taken in conjunction with the observation of intermolecular contacts in the solid-state structure of **5** would indicate the possibility of higher oligomers of these heterometallics in the gas phase. Only minimal amounts of organofluorine byproducts were detected.

Discussion

Metal–Fluorine Interactions. The above results indicate that to understand the structure and bonding in fluoroalkoxide metal complexes, metal–fluorine interactions in the solid state, solution, and/or gas phase must be considered. Given their long bond lengths in the solid state, these interactions are likely weaker than M–O bonds, yet long metal–halocarbon interactions have well-precedented effects on reactivity.[10a]

One method in which to understand the influences of these halocarbon contacts on the metal center is to make use of an overlap argument. One qualitative example is the concept of secondary bonding. This is the idea that while some ligands may not be direct bonded to the metal center (distances less than or equal to the combined covalent radii), they can significantly influence the bonding picture of the system at distances up to the sum of their van der Waals radii.[33] Secondary bonding has been observed for numerous metal–halocarbon systems, and in some cases been shown to substantially affect the general chemistry of the molecule. For fluorocarbon systems, examples of secondary bonding have been reported very recently for many of the alkali and the alkali earth elements[10a,34] as well as some transition[10a,35] and p-block metals.[10a,36] For sodium–fluorine systems, the realm of secondary bonding would lie between 2.27 Å ($F_{cov.}$ = 0.73 Å, $Na_{cov.}$ = 1.54 Å)[37] and 3.80 Å ($F_{v.d.W.}$ = 1.50 Å, $Na_{v.d.W.}$ = 2.30 Å).[38] For thallium, the distances are somewhat different, with a range from 2.28 Å ($Tl_{cov.}$ = 1.55 Å)[39] to 3.50 Å ($Tl_{v.d.W.}$ = 2.00 Å). This would imply that, at the same distance, sodium–fluorine interactions are stronger than thallium–fluorine interactions.

Chart I

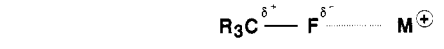

Sodium–fluorine interactions within the range mentioned above have been observed previously. The structure of sodium fluoroacetate shows Na^+–F contacts ranging from 2.47 to 2.56 Å,[40] well within the given threshold of secondary bonding. Sodium–fluorine interactions have also been seen in the species $Na_2Cu(OCH(CF_3)_2)_4$, where distances range from 2.481(7) to 2.791(7) Å.[41] In the systems reported here, comparable sodium–fluorine distances are observed. In the structure of **1**, 24 inter- and intramolecular distances of less than 3.80 Å are observed. In both **4a,b**, six fluorines approach each sodium at distances of less than the combined van der Waals radii.

Precedence for thallium–fluorine secondary bonding is less available. While numerous structures containing thallium and fluorocarbon ligands have been published,[42] little analysis of the Tl–F coordination sphere has been reported. One example is the interaction of a thallium(I) cation with the ortho fluorines of pentafluorothiophenolate ligands in the solid state with the average Tl–F distance being 3.062 Å.[26] In the structure of **5**, nine metal–fluorine contacts are found to occur within the combined van der Waals radii.

The overlap analysis neglects the electrostatic component of the system, an important consideration when considering halocarbon–metal interactions (Chart I). In the case of fluoroalkoxide systems, the electrostatic influences are of particular importance considering the polar nature of the carbon–fluorine bond (shown to have up to 43% ionic character[43]) and the highly ionic environment of the metal ion. Making use of valence bond sums,[44] the electrostatic influence the fluorines on the metal coordination sphere can be quantitatively measured. Valence bond sums (VBS) have been employed to analyze metal–organofluorine interactions in the solid state.[6] This method is based on ionic compounds in which the sum of the bond valences are roughly constant and should be near unity ($\sigma \approx 10\%$). Because of the ionic character of the carbon–fluorine bond, the VBS can be used to gain a rough approximation of the fluorine's influence on the metal ion. Since VBS are calculated using the ionic radii of the metals involved ($Tl^+_{12\ coord.}$ = 1.84 Å and $Na^+_{8\ coord.}$ = 1.32 Å),[45] contrary to overlap analysis, thallium–fluorine interactions would be expected to be stronger than those with sodium at equal distances. Making use of the Brown–Shannon formula[44a] ($S = (R/R_o)^{-N}$) and their values for R_o and N for sodium, thallium, oxygen, and fluorine,[6] the valence bond sums were calculated for the first coordination sphere[46] for all the species reported here (Table VIII). From these calculations, the importance of the electrostatic component of fluorine in completing the coordination shell of the metal can

(33) Alcock, N. W. *Adv. Inorg. Radiochem.* **1972**, *15*, 1.
(34) (a) Bradley, D. C.; Hasen, M.; Hursthouse, M. B.; Motevalli, M.; Khan, O. F. Z.; Pritchard, R. G.; Williams, J. O. *J. Chem. Soc., Chem. Commun.* **1992**, 575. (b) Bennet, M. J.; Cotton, F. A.; Legzdins, P.; Lippard, S. J. *Inorg. Chem.* **1968**, *7*, 1770. (c) Purdy, A. P.; George, C. F. *Inorg. Chem.* **1991**, *30*, 1970.
(35) Usón, R.; Fornies, J.; Tomás, M. *J. Organomet. Chem.* **1988**, *358*, 525.
(36) (a) Khan, L. A.; Malik, M. A.; Motevalli, M.; O'Brien, P. *J. Chem. Soc., Chem. Commun.* **1992**, 1257. (b) Edelmann, F. T. *Comments Inorg. Chem.* **1992**, *12*, 259. (c) Usón, R.; Fornies, J.; Falvello, L. R.; Usón, M. R.; Usón, I. *Inorg. Chem.* **1992**, *31*, 3697.
(37) Covalent radii from: Huheey, J. E. *Inorganic Chemistry*, 3rd ed.; Harper and Row: New York, 1983; Table G.1.
(38) Van der Waals radii from: Bondi, A. *J. Phys. Chem.* **1964**, *68*, 441.
(39) Emsley, J. *The Elements*; Clarendon Press: Oxford, U.K., 1989.
(40) Vedavathi, B. M.; Vijayan, K. *Acta Crystallogr., Sect. B* **1977**, *33*, 946.
(41) Purdy, A. P.; George, C. F.; Callahan, J. H. *Inorg. Chem.* **1991**, *30*, 2812.
(42) (a) Tachiyashiki, S.; Nakakyama, H.; Kuroda, R.; Sato, S.; Saito, Y. *Acta Crystallogr., Sect. B* **1975**, *31*, 1483. (b) Roesky, H. W.; Scholz, M.; Noltemeyer, M.; Edelmann, F. T. *Inorg. Chem.* **1989**, *28*, 3829.
(43) Sheppard, W. A.; Sharts, L. M. In *Organic Fluorine Chemistry*; Banjamin, W. A., Ed.; New York, 1969; p 19.
(44) (a) Brown, I. D.; Shannon, R. D. *Acta Crystallogr., Sect. B* **1973**, *29*, 266. (b) Brown, I. D.; Wu, K. K. *Acta Crystallogr., Sect. B* **1976**, *32*, 1957. (c) Donnay, G.; Allman, R. *Am. Mineral.* **1970**, *55*, 1003.
(45) Shannon, R. D. *Acta Crystallogr., Sect. A* **1976**, *32*, 751.
(46) Line-of-sight between oppositely charged atoms and cutoff chosen as $S \leq 0.010$.

Table VIII. Valence Bond Sums for Sodium- and Thallium-Containing Fluoroalkoxides

	M	R- (M–O)[a]	S- (M–O)[b]	R- (M–F)[a]	S- (M–F)[b]	ΣS
$(NaOR_f)_4$						
	Na(1)	2.264	0.239	2.365[c]	0.158	
		2.316	0.217	2.641	0.099	
		2.325	0.213	2.831	0.073	
				2.992	0.064	
				3.009	0.056	
				3.447	0.031	
				3.736[c]	0.022	
			0.669		0.503	1.172
	Na(2)	2.250	0.246	2.480[c]	0.129	
		2.255	0.243	2.652	0.097	
		2.296	0.225	2.993	0.058	
				3.379	0.034	
				3.750	0.022	
			0.714		0.340	1.054
	Na(3)	2.268	0.237	2.411[c]	0.146	
		2.301	0.223	2.635	0.100	
		2.315	0.217	2.636	0.099	
				2.745	0.084	
				3.471	0.031	
				3.640	0.025	
			0.677		0.485	1.116
	Na(4)	2.315	0.217	2.698	0.090	
		2.334	0.210	2.736	0.083	
		2.342	0.207	2.805[c]	0.076	
				2.857	0.070	
				3.375[c]	0.034	
				3.377	0.034	
				3.506	0.029	
				3.945	0.018	
			0.634		0.434	1.068
$Na_2Zr(OR_f)_6$-(C_6H_6)						
	Na	2.504×3	0.155×3	2.718×3	0.087×3	
				3.413×3	0.033×3	
			0.466		0.360	0.828
$Na_2Zr(OR_f)_6$-$(C_6H_6)_2$						
	Na	2.413×2	0.182×2	2.675×2	0.093×2	
				2.810×2	0.076×2	
				3.462×2	0.031×2	
			0.364		0.401	0.765
$(Tl_2Zr(OR_f)_6)_n$						
	Tl	2.740	0.203	3.135	0.066	
		2.814	0.173	3.215	0.057	
		2.831	0.167	3.238	0.054	
				3.096	0.071	
				3.068	0.075	
				3.289	0.050	
				3.289[c]	0.050	
				3.378[c]	0.042	
				3.442[c]	0.038	
			0.543		0.503	1.046

[a] Distances in Å. [b] $S=(R/R_o)^{-N}$ where: $R_o=1.622$ and $N=4.290$ for Na–O; $R_o=1.539$ and $N=4.290$ for Na–F; $R_o=2.100$ and $N=6.000$ for Tl–O; $R_o=1.993$ and $N=6.000$ for Tl–F. [c] Intermolecular interactions.

be seen, since the M–O contribution is frequently only half the total VBS; fluorines contribute the remainder. Moreover, by including the fluorine distances, the valence bond sums are significantly closer to unity than without. The only systems where the VBS do not approximately equal 1 are for **4a,b**, where the values for the benzene interactions were not included. This further supports the importance of these aromatic contacts.

Neither a purely overlap nor a purely electrostatic analysis of fluoroalkoxides will give a perfect model of the extent of interactions that occur between the metal and the fluorine. However, both are in agreement that these contacts are important in the overall bonding picture of these complexes.

The metal–fluorine interactions are found to also satisfy the geometric requirements of the metals involved. In each of the systems presented here with metals having extensive metal–fluorine contacts, the metal–oxygen coordination geometry is either trigonal pyramidal or two-coordinate bent. These geometries do not symmetrically balance the charge around the metal ion as compared to higher symmetry configurations, such as a tetrahedral or an octahedral environment, thus enhancing the electrophilicity of the M^+ ion. The electrophilicity of the metal ion is even further enhanced by the poor donor ability of the electron-deficient fluoroalkoxide oxygen.[4] As a result, the ligand-deficient (and electron-deficient) metal center binds fluorine both intra- and intermolecularly, or benzene in the case of **4a,b**. These contacts are enthalpically stabilizing and obviate the need for additional alkoxide bridging to fill the coordination sphere of the cation. Such alkoxide bridging is observed for $(Tl_2Sn(OEt)_6)_n$.[47]

Fluorine itself is a poor donor[10] due to its high electronegativity, but numerous weak fluorine interactions can help stabilize the positive charge of the metal. This stabilization does not require direct lone pair donation but can be Coulombic in nature, where the close intramolecular approach of the negatively-charged fluorines helps neutralize the charge of the M^+ ion. This effect may explain the enhanced volatility of fluorocarbon-based precursors. With the fluorines shielding the positive charge of the metal, intermolecular Columbic forces between the metal and oxygens of an adjacent molecule are reduced, thus increasing the volatility of the bulk material. Such shielding effects would be much less efficient in hydrocarbon analogues. The intermolecular metal–fluorine interactions reported here might be expected to decrease volatility. However, they may be readily replaced by intramolecular contacts, thus having little effect on volatility.

Solution Dynamics. The presence of the metal–fluorine interactions is exhibited by the ^{19}F–Tl coupling constants in the NMR studies of **5**. This coupling is relatively large considering the fact that it is dynamically distributed over 36 fluorines, as indicated by the triplet in the ^{19}F variable-temperature NMR spectra.[26] A mechanism for this fluxionality is postulated (Scheme I). Breaking one metal–oxygen bond with each thallium center, passing the thallium through the O–Zr–O plane, and reforming the bond with a new alkoxy oxygen would cause a new set of fluorine–metal interactions. Such a thallium migration process mimics *proton* migration seen in $M(OR)_x(HOR)_y$ systems and would accomplish equivalency of the fluorine atoms on the NMR time scale. Complex **4** is likely to have a fluxional mechanism similar to that of **5**. In the case of **4**, due to the smaller ionic radii of the M^+ ion, the dynamic process would be more facile. Thus, fluxional spectra are observed at room temperature. Insight can be obtained on the overall mechanism by reexamination of the structures of **4a,b**. In the case of **4b**, one alkoxide fails to bridge to sodium. This structure represents the dissociative first step (**A**) of the proposed $Tl_2Zr(OR_f)_6$ fluxional mechanism. This would indicate that such a process is of low energy, being present in the solid state. Further analysis of the two heterometallic systems reveal both to have metal–fluorine secondary bonding contacts. Taking into account the larger ionic radius of thallium, the metal–fluorine interactions for sodium and thallium are comparable. Given the nuclear spin coupling observed in **5**, attractive sodium–fluorine interactions in **4** are likely to be of a similar magnitude.

Carbon–Fluorine Bond Cleavage. The metal–fluorine interactions observed in these fluoroalkoxide complexes may assist in carbon–fluorine bond cleavage. Metal activation of C–F bonds has been previously observed, but usually with zero-valent metal systems and highly activated fluorocarbons.[48] Fahey and Mahan have shown that $(COD)Ni(PEt_3)_2$ (COD = cyclooctadiene) in the presence of the strong electrophile hexafluorobenzene with

(47) Hampden-Smith, M. J.; Smith, D. E.; Duesler, E. N. *Inorg. Chem.* **1989**, *28*, 3399.

extended heating will produce *trans*-$(PEt_3)_2NiF(C_6F_5)$ in very low yield.[49] Cleavage of unsaturated fluorocarbons is also observed in the reaction of the strongly reducing Cp^*_2Yb with a variety of fluorinated alkene and alkyne reagents producing Cp^*_2YbR and the mixed valence $[Cp^*_2Yb]_2F$.[50] One of the few examples of attack at the C–F bond in a saturated system is the reaction of Mg^0 with fluorohexane producing RMgF.[51] However, for the systems we report here, oxidative addition mechanisms for cleavage of the C–F bond are not viable. However, all these compounds produce metal fluorides in the mass spectrometer and $(NaOR_f)_4$ produces nearly exclusively NaF under CVD conditions. Thermodynamics can play a major role since MF_x (M = Zr, Tl, Na) is thermodynamically more stable than the corresponding oxides.[52] Yet for this process to occur, the kinetic barrier for the cleavage of the stronger C–F with respect to the C–O bond must be overcome ($\Delta H°$ = 116 kcal/mol *vs* $\Delta H°$ = 88 kcal/mol for C–O). The secondary interaction of fluorine with the metal in the molecular precursor may reduce this kinetic barrier, weakening the C–F bond and assisting in fluorine transfer. Note that C–F bonds involved here in secondary bonding are not lengthened perceptibly, but C–X bond lengthening is also absent for coordinated R_3CX, yet reactivity toward C–X cleavage is enhanced by many orders of magnitude.[10] This also does not preclude other interactions and distortions under CVD or mass spectrometer conditions (gas phase). Under such conditions, intermolecular C–F interactions are absent and the electrophilic nature of the sodium ion would be enhanced, potentially increasing the intramolecular sodium–fluorine interactions. Even if the C–F bond is not weakened by fluorine interaction with the metal, the coordination of fluorine to the sodium is a necessary first step in the eventual cleavage of the covalent bond, which is observed for the systems reported here. In contrast, the compound $(NaO^iPr)_n$ does not decompose until temperatures greater than 400 °C.[53] This is consistent with the idea that Na–F contacts in the structure provide a low-energy decomposition mechanism.

Future mechanistic investigations must decipher the specific pathway involved in the formation of the metal fluorides, as well as CVD studies of the other fluoroalkoxide species reported here.

Conclusions

In the above work, a variety of fluoroalkoxide compounds have been prepared and studied. In general, these species exhibit greater volatility than normal hydrocarbon-based systems. However, in the solid state, solution, and presumably the gas phase, M–F interactions are observed. These interactions provide a kinetic route to metal fluoride products (rather than oxides, the expected material based on the direct metal–oxygen bonding present in the precursor). It should be noted that while fluorine contamination of oxide films is undesirable, pure metal fluorides have many desirable properties of their own. CaF_2[54] and BaF_2[55] are used in thin-film scintillator devices,[56] NaF is found to be an excellent protective coating for optical devices,[57] and mixed-metal fluoride glasses are used in high-energy optical applications.[58] Thus, while optimization of the fluoroalkoxide systems to produce pure metal oxides is important, production of pure metal fluoride films has its own relevance. More work is needed to establish products and the mechanism of decomposition in order to gain a better understanding of how to design an effective precursor.

The weight of evidence here that carbon-bound fluorine is sufficiently electron-rich to interact with electrophilic metal cations expands and reinforces the evidence that such fluorines are willing electron pair donors in hydrogen bonds.[6,48a]

Acknowledgment. We thank Professor David V. Baxter, Eyal H. Barash, Bryan E. Hauger, and Dr. Ulrike Werner for helpful discussions and technical assistance, AMOCO Research Corp. for the donation of an NMR spectrometer, and the Department of Energy for funding.

Supplementary Material Available: Tables of mass spectra crystallographic data, fractional coordinates, full bond lengths and angles, isotropic and anisotropic thermal parameters, and mass spectral analysis data for **1**, **3**, **4a,b**, and **5**, discussion of NMR experimental details, and drawings of the disorder in **3** (37 pages); listings of structure factors (36 pages). Ordering information is given on any current masthead page.

(48) (a) For a general review of hydrogen bonding to F and of metal-mediated C–F bond cleavage, see: Richmond, T. G. *Coord. Chem. Rev.* **1990**, *105*, 221. (b) Crespo, M.; Martinez, M.; Sales, J. *J. Chem. Soc., Chem. Commun.* **1992**, 822.

(49) Fahey, D. R.; Mahan, J. E. *J. Am. Chem. Soc.* **1977**, *99*, 2501.

(50) Anderson, R. A.; Burns, C. J. *J. Chem. Soc., Chem. Commun.* **1989**, 136.

(51) Ashby, E. C.; Yu, S. H.; Beach, R. G. *J. Am. Chem. Soc.* **1970**, *92*, 433.

(52) $\Delta G_f^°$ (kcal/mol): –456.8 (ZrF_4 (β, monoclinic)), –249.24 (ZrO_2 (α, monoclinic)), –74.38 (TlF), –35.2 (Tl_2O), –129.902 (NaF), –89.74 (Na_2O). See: *Handbook of Chemistry and Physics*, 66th ed.; Weast, R. C., Ed.; CRC Press Inc.: Boca Raton, FL, 1985; pp D51–93.

(53) Chisholm, M. X.; Xue, Z. B. Personal communication.

(54) Winn, D. R.; Lapierre, C.; Whitmore, M.; Kirlin, P.; Binder, R. *IEEE Trans. Nuc. Sci.*, in press.

(55) Korner, H. J. *Bull. Am. Phys. Soc.* **1988**, *33*, 1091.

(56) Kirlin, P. S.; Binder, R.; Winn, D. R.; O'Hare, J.; LaPierre, L.; Whitmore, M. *Nucl. Instrum. Methods Phys. Res.* **1990**, *A289*, 261.

(57) Zwedowski, S.; Andrze, J. *Opt. Appl.* **1987**, *17*, 363.

(58) (a) Izumitani, T.; Tokita, M.; Yamashita, T.; Miura, S. JPN Patent 62256740, 1986, 6 pp. (b) Hirai, S.; Yoshiki, C. JPN Patent 63248737, 1988, 7 pp.